analytical chemistry

pubs.acs.org/ac Article

Label-Free and Sensitive Electrochemical Biosensor for Amplification Detection of Target Nucleic Acids Based on Transduction Hairpins and Three-Leg DNAzyme Walkers

Yu Xue, Yu Wang, Sinuo Feng, Mengxia Yan, Jianshe Huang,* and Xiurong Yang*

Cite This: *Anal. Chem.* 2021, 93, 8962−8970 Read Online

ACCESS | Metrics & More | Article Recommendations | Supporting Information

ABSTRACT: Nucleic acids are regarded as reliable biomarkers for the early diagnosis of various diseases. By ingeniously combining a transduction hairpin (THP) with the toehold-mediated strand displacement reaction (TSDR) to form three-leg DNAzyme walkers, for the first time, we constructed a label-free and sensitive electrochemical sensing system for the amplification detection of target nucleic acids. With microRNA-155 (miR-155) as a model target, the feasibility of the biosensing strategy and the conformational states of DNA in the recognition process were studied in detail on the basis of electrochemical and dual polarization interferometry techniques. With the assistance of THP, miR-155 indirectly triggered the TSDR between three hairpins (H1, H2, and H3), then massive Mg^{2+}-dependent three-leg DNAzyme walkers were formed in aqueous solutions. After the binding/cleaving/moving process of three-leg DNAzyme walkers on the electrode surface modified with substrate hairpins (SHPs), a number of single-stranded DNAs (ssDNAs) were generated. Hence, the interaction of methylene blue (MB) with the duplex section of SHPs was impeded, which brought about a decreased electrochemical signal. Benefiting from the cyclic amplification of the TSDR and the higher cleavage activity of three-leg DNAzyme walkers, the proposed sensing strategy showed remarkable improvement in sensitivity with a low detection limit of 0.27 fM for miR-155. Owing to the precise design of the THP, this method exhibited excellent specificity to distinguish miR-155 from the single-base and triplex-base mismatched sequences. This sensing strategy importing the flexible THP can be utilized to detect various nucleic acid biomarkers by only redesigning the THP without changing the main circuit or reporter constructs, showing the great versatility and potential for the early diagnostics and biological analysis.

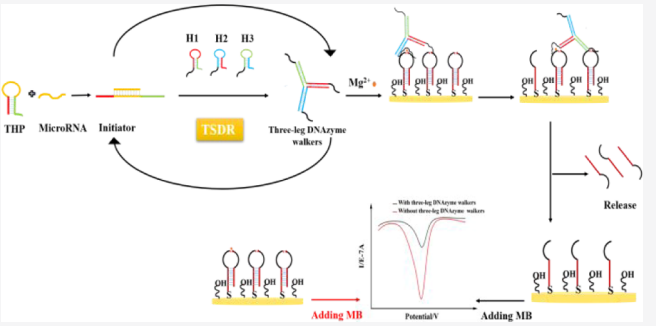

MicroRNAs, a class of typical nucleic acid biomarkers, play critical roles in the regulation of various biological processes including cellular proliferation, differentiation, and apoptosis.[1] Some human diseases are intimately associated with their abnormal expression.[2,3] MicroRNA-155 (miR-155), for example, is a typical multifunctional microRNA which is involved in many biological processes, such as gene (mRNA) expression, development of cellular phenotypes, and normal erythroid differentiation.[4−6] The expression patterns of miR-155 are closely related to neurodegenerative diseases.[7] Hence, considerable efforts have been devoted to constructing a series of amplification strategies to sensitively and specifically analyze the nucleic acid biomarkers with a low-level expression in real samples.[8−10]

The toehold-mediated strand displacement reaction (TSDR), which has been proved to be an effectively isothermal DNA amplification strategy, is a key mechanism in DNA nanotechnology.[11−13] In this mechanism, a short single-stranded overhang region (termed toehold) facilitates the branch migration process and the strand displacement reaction on a duplex helix.[14] Based on the toehold exchange mechanism, multifarious DNA nanostructures have been reported by the way of the target-triggered and entropy-driven self-assembly of metastable hairpins.[15−18] Due to the recycling utilization of a target sequence in TSDR, a great number of DNA nanostructures are generated, providing 100-fold amplification of the target-triggered hybridization event.[19,20]

A transduction hairpin (THP), which has the stem-loop structure, is a single-stranded oligonucleotide hybridization probe. The sequence of loop and stem is designed specially to implement the transduction function. First, the loop is designed to be complementary to the target sequence and the stem is designed to seal the toehold of following isothermal amplification reactions.[21] In the presence of the target sequence, it completely hybridizes with the loop region.

Received: April 10, 2021
Accepted: June 7, 2021
Published: June 16, 2021

https://doi.org/10.1021/acs.analchem.1c01522
Anal. Chem. 2021, 93, 8962−8970

Therefore, the THP is opened and the toehold is exposed for the next isothermal amplification reaction. That is to say, in terms of a cyclic amplification detecting system where the THP was used as a converter, only the sequence of the THP needs to be changed for detecting different target genes, which simplify the design process to detect different target sequences. Li and co-workers have successfully optimized the design method of THPs and detected the loop-mediated isothermal amplification of DNA by combining the THP with the enzyme-free DNA circuits.[21,22]

DNAzymes, the functionally active and synthetic single-stranded DNA (ssDNA), possess the catalytic ability toward chemical reactions, which is similar to that of RNAzyme and protease. The selected metal ion-dependent DNAzymes are composed of a central catalytic domain and a two-arm sequence. With the assistance of metal-ion cofactors, DNAzymes could cleave the substrate by the catalytic domain and the two arms.[23,24] In view of their flexibility of design, simplicity of modification, and excellent catalytic ability, the application of DNAzyme-based gene silencing has been explored in a broad range, especially in sensing and biomedical devices.[25−27] DNA walkers are DNA machines that can autonomously move along the nucleic acid "track" under the motivation of strand displacement strategies or cleavage site.[28] Huang groups,[29] for example, have designed a electrochemical biosensor for the ultrasensitive detection of ochratoxin A, which utilize the strand displacement-driven super-fast tripedal DNA walker to transduce and amplify the electrochemical signals. Moreover, some previous reports have applied DNAzymes to stimulate DNA walkers by virtue of their excellent cleavage activity toward substrates. Based on the autonomous motion and superior controllability of DNAzyme walkers, various applications, such as developing biosensors, diagnostic systems, drug delivery, and molecular transports, have been implemented.[30−33]

Taking the above advantages into account, a label-free and sensitive electrochemical biosensor was constructed for the first time by tactfully integrating a THP with a toehold-mediated stand displacement reaction (TSDR) to form three-leg DNAzyme walkers. In this sensing system, miR-155 is selected as the target microRNA. When target miR-155 is introduced into the sensing system, the THP is opened specifically, which triggers the next TSDR and finally forms the three-leg DNAzyme walkers. After one cycle of TSDR, the hybridization products (miR-155/THP) are released. Therefore, the TSDR process is cycled to generate numerous three-leg DNAzyme walkers, and the input signal of miR-155 is amplified. Whereafter, the three-leg DNAzyme walkers are applied to recognize and cleave substrate hairpins (SHPs) immobilized on the electrode surface to produce massive ssDNA, which rendered the declined the electrochemical signal of methylene blue (MB). Because of the cycle amplification ability of TSDRs and the admirable catalytic activity of three-leg DNAzyme walkers, the sensitivity of the proposed biosensor is greatly improved, showing a limit of detection (LOD) as low as 0.27 fM for miR-155. At the same time, the subtle design of THPs guarantees the strict recognition of miR-155 against other interference sequences. The developed method shows a promising prospect of application for nucleic acid diagnostics and analysis.

EXPERIMENTAL SECTION

Reagents and Apparatuses. The chemicals and apparatuses used in this work are shown in the Supporting Information and the sequences of all DNAs and RNAs are listed in Table S1.

Construction of the Three-Leg DNAzyme Walkers. A THP was designed according to a previous report.[22] The hairpin probes H1, H2, and H3 were designed based on the principle of the enzyme-free strand-displacement nucleic acid circuit system. The SHP whose stem was rich in guanine and cytosine was devised specially. Prior to the experiments, each kind of hairpin probe (THP, SHP, H1, H2, and H3) was heated at 95 °C for 5 min and then slowly cooled to 25 °C for at least 2 h, assuring that the DNAs hold stable secondary structures and hybridize effectively with other DNAs. The annealed DNAs were stored at 4 °C for further use. After the annealing process, the THP (50 nM), H1 (50 nM), H2 (50 nM), and H3 (50 nM) were blended with different concentrations of miR-155 in TNKM buffer (20 mM Tris−HCl, 140 mM NaCl, 5 mM KCl, and 20 mM $MgCl_2$; pH 7.5), reacting at 25 °C for 120 min to form the three-leg DNAzyme walkers.

Electrochemical Sensing Process. The cleaning procedure of the gold electrode (GE) is as follows: first, the gold electrode was soaked in piranha solution (30% H_2O_2 and 98% H_2SO_4 at a volume ratio of 1:3) for 30 min. Then, the GE was rinsed with double-distilled water and further cleaned by successively polishing with 0.3 and 0.05 μm alumina slurry, followed by continuous sonication in ethanol and double-distilled water three times, respectively. Finally, electrochemical cleaning was performed in 0.5 M H_2SO_4 until the characteristic cyclic voltammetry (CV) curve was obtained. A thiol-terminated SHP (1 μM) was incubated with TCEP (1 mM) for 1 h at room temperature to break the disulfide bond. Then, the TCEP-pretreated SHP (8 μL, 1 μM) was dropped on the GE overnight at 4 °C to prepare the SHP/GE. Subsequently, 8 μL of 6-mercapto-1-hexanol (MCH; 1 mM) in TNKM buffer was cast on the electrode and incubated at 4 °C for 1 h to block the unreacted Au sites; the modified electrode was named MCH/SHP/GE. After that, 8 μL of the reaction mixture (THP + H1 + H2 +H3 + miR-155) was dropped onto MCH/SHP/GE and incubated at 25 °C for 30 min. Eventually, the binding of MB with the SHP on the electrode surface was performed in TN buffer (20 mM Tris−HCl and 20 mM NaCl; pH 7.0) containing 0.2 mM MB for 20 min. It is noted that the electrode was rinsed thoroughly with TNT buffer (20 mM Tris−HCl, 150 mM NaCl, and 0.05% Tween 20; pH 7.5) and TNKM buffer after each step of modification. The differential pulse voltammetry (DPV) measurement was executed in TN buffer with a pulse width of 0.05 s, a sampling width of 0.0167 s, a pulse amplitude of 0.01 V, and a scanning range from 0.1 to −0.5 V.

Native Polyacrylamide Gel Electrophoresis. A total volume of 10 μL of different reaction solutions mixed with loading buffer (6×) was loaded into the lanes of 10% polyacrylamide gel electrophoresis (PAGE) in 1× TBE (89 mM Tris-Boric Acid, 2 mM EDTA) buffer for the electrophoresis experiment.

Dual Polarization Interferometry Measurements. For the dual polarization interferometry (DPI) experiment, the first step is to prepare the amino-modified sensor chip as reported previously.[34] The bare silicon oxynitride AnaChip was first

https://doi.org/10.1021/acs.analchem.1c01522
Anal. Chem. 2021, 93, 8962−8970

Scheme 1. Schematic Diagram of the Proposed Electrochemical Biosensor for MicroRNA Detection Based on the THP and Three-Leg DNAzyme Walkers

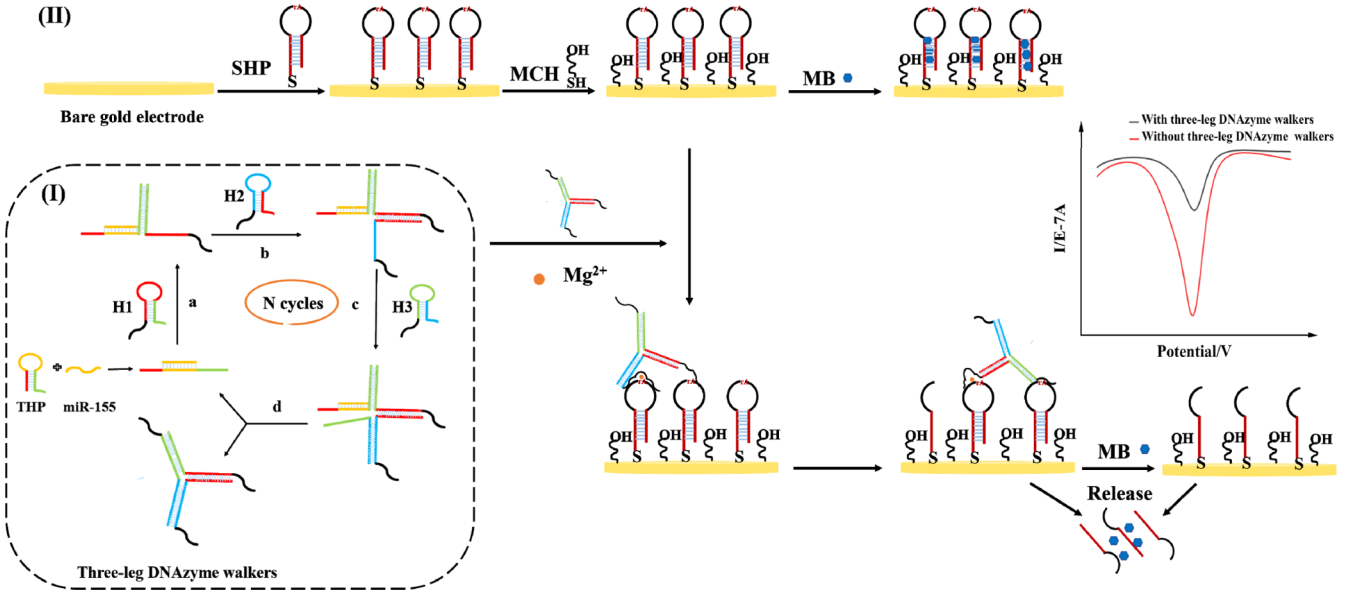

cleaned with Piranha solution at room temperature for 12 h. Next, the chip was cleaned by sonicating in ultrapure water for 6 min; this procedure was repeated six times. Then, the dried bare chip was aminated by immersing in 10% (3-Aminopropyl)trimethoxysilane at 30 °C for 2 h. Finally, the amino-modified sensor chip was washed thoroughly with ultrapure water and ethanol, respectively, and dried with a stream of nitrogen.

In this work, 10 mM PBS solution (137 mM NaCl, PH 7.4) served as the running buffer for all the DPI experiments. The calibration and linearization processes were the same as those of previous reports.[35,36] After calibrations, the flow rate was kept at a constant rate of 50 μL/min. When a stable baseline appeared, 250 μL of GA (1%) was injected at 50 μL/min for 5 min. Next, a 250 μL amine-modified SHP (6 μM) was injected for 1 min at 50 μL/min and then 10 μL/min for 10 min. The reaction mixture of THP, H1, H2, H3, and miR-155, containing three-leg DNAzyme walkers, was sequentially injected into each channel at 8 μL/min. When all of the samples were loaded and the baseline was steady, the experiment was stopped. All experimental data were converted into a refractive index, thickness, mass, and density values and analyzed by AnaLight DAQ software.

Atomic Force Microscopy. Ten microliters of the DNA reaction products (5 μM) were diluted in TNKM buffer and dropped onto the freshly cleaved mica for 5 min. Then, the samples were rinsed with deionized water and dried with nitrogen. Finally, atomic force microscopy (AFM) imaging experiments were conducted on a Dimension Edge atomic force microscope (Bruker, Germany) in air under tapping mode.

RESULTS AND DISCUSSION

Design Principle of the Sensing Strategy for Nucleic Acid Detection. Taking miR-155 as an example, the principle of the proposed sensing strategy is illustrated in Scheme 1. The sensing process of this system is divided into two steps including homogeneous reaction (I) and heterogeneous reaction (II). The homogeneous reaction includes three hairpin probes (H1, H2, H3) and THP. H1, H2, and H3 probes contain the Mg^{2+}-dependent DNAzyme sequence at the 5′ end (the black section). The THP is designed especially to have 22 nt in the loop region, which can hybridize with target miR-155, and 10 base pairs in the stem region that lock the catalytic site for TSDR. When miR-155 is added into the reaction solution, it primarily hybridizes with the complementary sequence in the THP (the yellow section) to unfold the THP. The toehold sealed in the THP (the green section) is exposed. Then, branch migration opens H1 and forms the miR-155-THP-H1 complex. H2 attaches to H1 via the toehold in opened H1 (the red section), initiating another branch migration reaction and ultimately forming the complex (miR-155-THP-H1-H2). When the toehold is opened in H2 (the blue section), H3 is opened as well. By now, all hairpins are opened and form the intermediate products (miR-155-THP-H1-H2-H3), which are thermodynamically unstable. With the exposed toehold in H3 (the green section) binding to H1, the stable three-leg DNAzyme walkers generated through the stand displacement reaction and the miR-155/THP complexes are released.[37] The released miR-155/THP complexes after one TSDR are capable of triggering the TSDR of H1, H2, and H3 in succession. This cyclic process produces plenty of three-leg DNAzyme walkers, which realizes the signal amplification of the inputted target miR-155.

After finishing the TSDR in homogeneous reaction solution, the heterogeneous reaction on the electrode surface is executed. Methylene blue (MB), an aromatic heterocycle that selectively intercalates in the DNA double helix, is selected as the electrochemical indicator.[38] Initially, the SHP, modified with a ribonucleobase recognition site at the loop region and a thiol group at the 3′ terminus, is immobilized on the gold electrode surface through a Au−S bond. Subsequently, three-leg DNAzyme walkers in the homogeneous reaction solution are dropped on the electrode to hybridize with SHP by the complementary bases in DNAzyme sequences. With the assistance of Mg^{2+}, SHP is split into two fragments at the ribonuclease recognition sites, resulting in the SHP changing from a stem-loop structure to ssDNA. Along with the

https://doi.org/10.1021/acs.analchem.1c01522
Anal. Chem. 2021, 93, 8962−8970

dissociation between cleaving fragments and DNAzymes, the recognition regions in DNAzymes are reactivated. Therefore, the DNAzymes can quickly explore another adjacent substrate site to attach to. Under the strand displacement driven by branch migration, the three-leg DNAzyme walkers find another SHP to bind to, cleave, and substitute, contributing to the higher efficiency movement of the walkers and the formation of numerous ssDNA on the electrode surface.[29] Hence, MB is unable to insert into the double-stranded sections of the SHP, which leads to generating weak electrochemical signals. Thus, a label-free and sensitive electrochemical biosensor was constructed for miR-155 detection.

Characterization of Three-Leg DNAzyme Walkers. For this sensing system, the formation of three-leg DNAzyme walkers by adding target miR-155 is vital. As shown in Figure 1, the hybrid product of miR-155 and THP (lane 3) shows an obviously decreased electrophoretic mobility compared with miR-155 (lane 1) and THP (lane 2), respectively, suggesting that the miR-155/THP complexes are formed. For the control experiment in which target miR-155 does not exist in the reaction solution containing THP, H1, H2, and H3, clear electrophoretic bands having a mobility similar to that of a single hairpin are observed (lane 7). On adding miR-155 to the reaction solution, a much brighter band exhibiting lower mobility is displayed in lane 9. In order to identify the formation of three-leg DNAzyme walkers, three hairpin DNAs (H1 + H2 + H3) are annealed to form the three-stranded Y-shaped complex (lane 8). We can clearly see that the products in lane 8 and lane 9 have the same molecule weight, which verifies the successful self-assembly formation of three-leg DNAzyme walkers in lane 9.

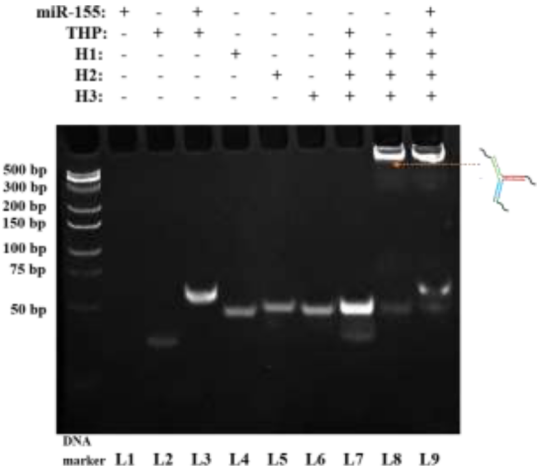

Figure 1. Native PAGE analysis of various reaction mixtures and three-leg DNAzyme walkers. Lanes 1−6: miR-155, THP, miR-155 + THP, H1, H2, H3, respectively; lane 7: H1 + H2 + H3 + THP; lane 8: the mixture of H1, H2, and H3 after the annealing process; lane 9: lane 7 + miR-155 to form three-leg DNAzyme walkers. The initial concentration of each DNA species is 10 μM.

The assembled products were further confirmed by AFM. From Figure S1A, in the absence of miR-155, there are only some tiny spots which might represent the unassembled substrates, indicating no sign of the assembly event. However, in the presence of miR-155, a uniform and compact surface morphology appears (Figure S1B). The presented surface morphology is good proof that the three-leg DNAzyme walkers are formed as anticipated,[39] which is coincident with the results obtained by PAGE (Figure 1).

CV and EIS Characterization of the Assembly Procedure on an Electrode. As shown in Figure 2A,B, CV and EIS were performed in $K_3[Fe(CN)_6]$ solution to demonstrate the validity of each modification step on the electrode surface. The diameter of all Nyquist plots in Figure 2B represent the electron transfer resistance (R_{et}) at the electrode surface. It can be seen that the bare GE showed a pair of well-defined redox peaks (Figure 2A, curve a) and a small R_{et} of about 16.3 Ω (Figure 2B, curve a). When SHP and MCH were immobilized on the electrode step-by-step, the peak current of SHP/GE and MCH/SHP/GE (Figure 2A, curve b and c) declined sequentially. Also, the R_{et} increased to 2330 and 6702 Ω (Figure 2B, curves b and c), respectively, which was ascribed to the repulsion of negative charges on the phosphate skeletons of the SHP to the $[Fe(CN)_6]^{3-/4-}$ pair and the hindrance to the electrochemical probe diffusion of the compact self-assembled layer of MCH. When the TSDR system without miR-155 was incubated with the MCH/SHP/GE, the modified electrode showed a peak current and an R_{et} (6404 Ω) similar to those of MCH/SHP/GE (curve d in Figure 2A,B). However, with the addition of miR-155 in the TSDR system, the peak current of the modified electrode increased obviously and the R_{et} decreased remarkably to 3778 Ω (curve e in Figure 2A,B). The reason is that the three-leg DNAzyme walkers could effectively cleave the SHP to produce ssDNA on the electrode surface, leading to the decreased

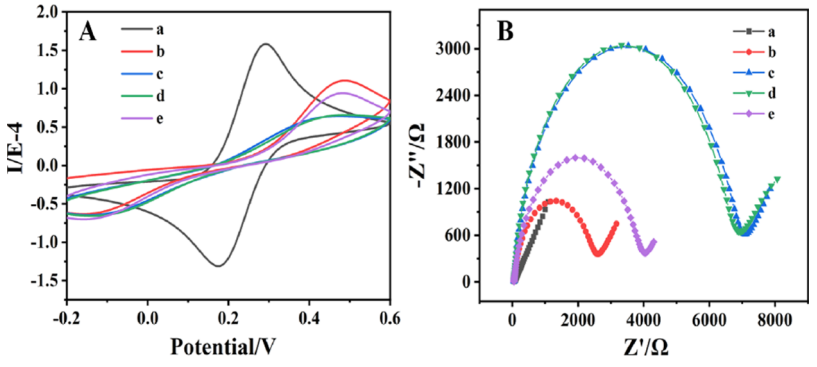

Figure 2. CV (A) and EIS (B) characterization results in 0.1 M KCl solution containing 5.0 mM $[Fe(CN)_6]^{3-/4-}$ at the bare GE (a), SHP/GE (b), MCH/SHP/GE (c), (H1 + H2 + H3 + THP + Mg^{2+}) incubated with MCH/SHP/GE (d), and (H1 + H2 + H3 + THP + miR-155 + Mg^{2+}) reacted with MCH/SHP/GE (e). Potential range: −0.2−0.6 V; scan rate: 100 mV s^{-1}; and frequency range: 0.1 to 10^5 Hz.

https://doi.org/10.1021/acs.analchem.1c01522
Anal. Chem. 2021, 93, 8962−8970

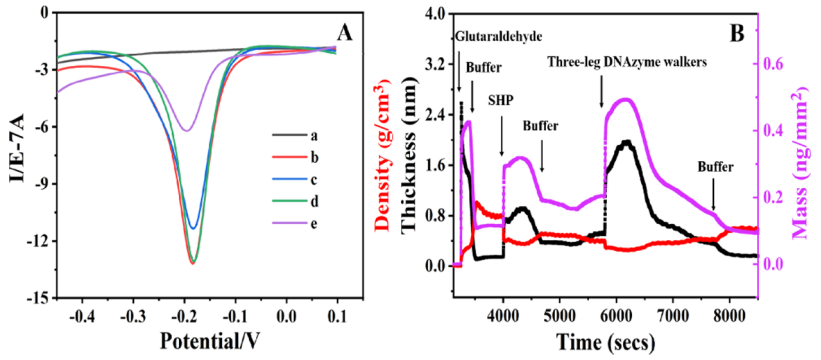

Figure 3. DPV curves (A) and real-time DPI characterization curves (B) to demonstrate the feasibility of the biosensor. (a) MCH/SHP/GE, (b) MB/MCH/SHP/GE, (c) MB/(THP + H1 + H2 + miR-155 + Mg^{2+})/MCH/SHP/GE, (d) MB/(THP + H1 + H2 + H3 + Mg^{2+})/MCH/SHP/GE, and (e) MB/(THP + H1 + H2 + H3 + miR-155 + Mg^{2+})/MCH/SHP/GE.

repulsive interaction between negatively charged SHP and the $[Fe(CN)_6]^{3-/4-}$ pair. The CV and EIS results not only confirmed the successful assembly processes but also preliminarily proved the viability of this sensing strategy. XPS analysis of the modified electrode surface was also performed, and the results verified the successful assembly and the cleaving of the SHP by DNAzymes (Figure S2).

Feasibility of the Biosensor. In order to ensure the feasibility of this biosensor, DPV measurements and DPI characterizations were carried out. As illustrated in Figure 3A, MB/MCH/SHP/GE exhibited the sharp MB reduction peak around −0.2 V after binding MB molecules (curve b). On account of that, MB inserted itself into the double-helix section of the SHP, realizing the transition of electrons from the electrode surface to MB.[40] After the three-leg DNAzyme walkers formed in the homogeneous solutions incubated with the MCH/SHP/GE, a remarkable decrease of peak current was observed (curve e). In contrast, in case of the modified electrodes incubated with the two-way DNAzyme walkers (THP-miR-155-H1-H2) (curve c) or the single DNAzyme molecules (H1, H2, H3) (curve d), the peak currents had only slight or ignorable changes, respectively. This result demonstrated that the three-leg DNAzyme walkers with multiple Mg^{2+}-dependent DNAzyme structures had higher cleavage efficiency compared with the two-way DNAzyme walkers and single DNAzyme molecules, which could not quickly recognize and bind to a contiguous site.[41] In addition, PAGE and fluorescence spectra analysis were also executed to testify the feasibility of this designed biosensor and the high cleavage activity of three-leg DNAzyme walkers. As displayed in Figure 4, the stripe of the SHP faded away after incubating with three-leg DNAzyme walkers and Mg^{2+} (lane 3). In addition, a new band with a fast move rate and a low molecular weight appeared, representing the cleaving fragments of the SHP. However, when the SHP was incubated with single DNAzyme molecules (lane 5) or two-way DNAzyme walkers (lane 6), the stripes of the SHP showed a negligible change or were slightly dim. The fluorescence experiment also confirmed the cleaving activity of three-leg DNAzyme walkers using SYBR Green I as the dsDNA-specific fluorescence probe (Figure S3). These results proved the higher cleavage activity of three-leg DNAzyme walkers, and the amplification strategy based on the THP and three-leg DNAzyme walkers to detect target nucleic acids could be implemented.

DPI, an evanescent optical biosensing platform, could offer the quantitative information and the real-time kinetic

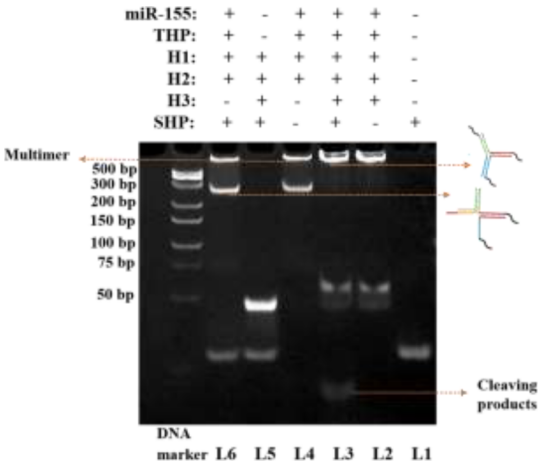

Figure 4. PAGE analysis of the feasibility of the developed method and the catalytic ability of different types DNAzyme. Lane 1: SHP; lane 2: THP + miR-155 + H1 + H2 + H3; lane 3: lane 2 + SHP; lane 4: miR-155 + THP + H1 + H2; lane 5: H1 + H2 + H3 + SHP; lane 6: lane 4 + SHP. The types of DNAzyme in lanes 3, 5, and 6 are three-leg DNAzyme walkers, single DNAzyme molecules, and two-way DNAzyme walkers, respectively.

conformation information related to the biomolecule interactions.[42] The DPI technique, for instance, has been applied to study the real-time interaction of DNA−small molecules, DNA−protein, and protein−protein.[43−45] Hence, real-time DPI experiments were carried out to further verify the feasibility of the designed biosensor. The conformation parameters (thickness, mass, and density values) and the biomolecular states on the chip surface were analyzed.[36] The typical DPI-sensorgrams are depicted in Figure 3B, and the detailed parameter values for each immobilized layer are shown in Table S2. When GA was introduced into the amine-modified chip, the thickness, mass, and density increased quickly. All the parameters declined and reached a stable value after reintroducing the running buffer, meaning that GA had been successfully immobilized on the chip surface and achieved a saturated state. Then, amino-SHP was immobilized on the chip surface by crosslinking with GA. After the injection of the SHP solution, the thickness and mass increased while the density decreased compared to the GA layer, indicating that the SHP was immobilized on the chip surface with a free state. When the reaction solution containing three-leg DNAzyme walkers was injected onto the DPI chip surface,

https://doi.org/10.1021/acs.analchem.1c01522
Anal. Chem. 2021, 93, 8962−8970

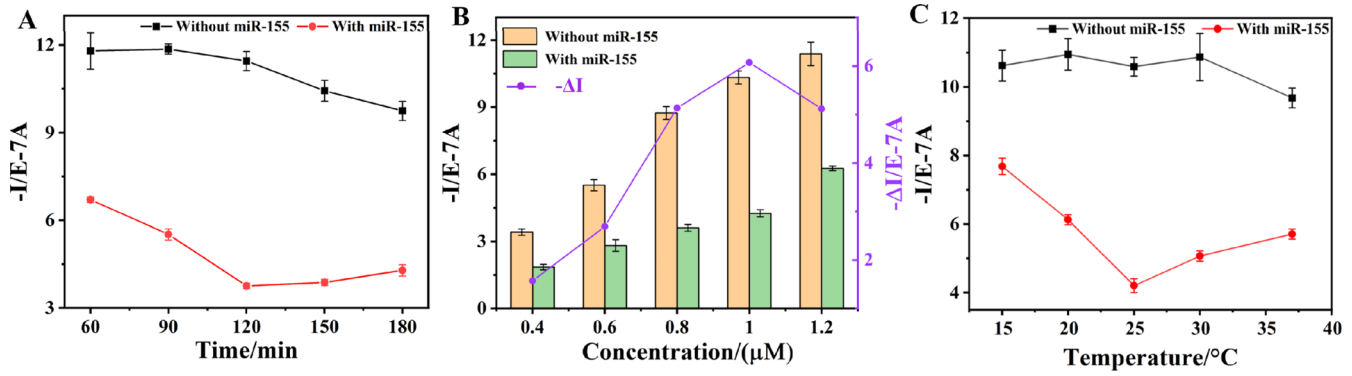

Figure 5. Optimization of assay conditions for the electrochemical detection of miR-155. Reaction time of the TSDR (A), the concentration of the SHP (B), and the reaction temperature for DNAzymes (C). The concentration of miR-155 in all experiments is 500 pM. Error bars show standard deviations of the three repeated experiments.

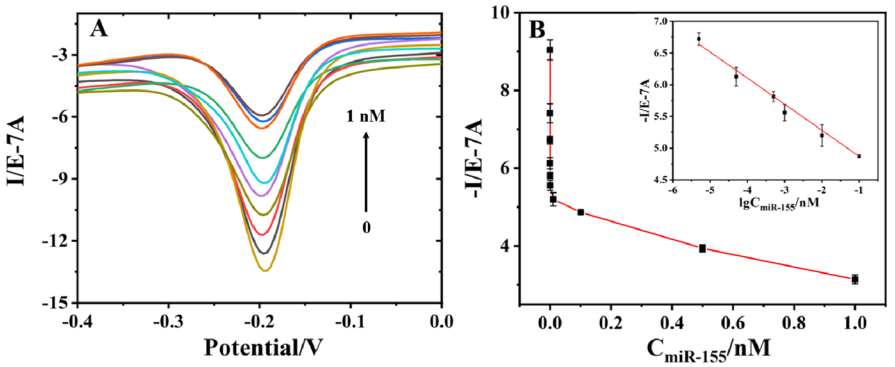

Figure 6. (A) DPV responses of the biosensor to different concentrations of miR-155 from 0 to 1 nM (0, 1 fM, 5 fM, 50 fM, 500 fM, 1.0 pM, 10 pM, 100 pM, 500 pM, and 1 nM). (B) Plot of the peak current intensity vs $C_{miR\text{-}155}$, and the inset shows the linear relationship between the peak current intensity and lg $C_{miR\text{-}155}$. Error bars represent the standard deviations of triplex experiments.

the thickness and mass increased and the density declined at the initial injection period. With prolonging the reaction time, however, the mass and thickness of the layer decreased continuously and the density increased gradually to a stable value. This phenomenon was ascribed to the SHP being cleaved into two fragments by three-leg DNAzyme walkers, and one part of these fragments were washed away from the chip surface by buffer solutions. The increase of density in the final step demonstrated that the remaining ssDNA on the chip surface existed in the form of random coils. Finally, the injection of running buffer terminated the cleavage reaction, and all parameters reached stable values. The DPI characterization not only demonstrated the feasibility of the heterogeneous reaction process in the sensing strategy but also showed the conformational state of DNA at each reaction step on the substrate surface.

Optimization of Experimental Conditions. For the sake of obtaining the best analytical performance and maximizing the sensitivity, several important assay parameters such as the reaction time of the TSDR, the concentration of the SHP, and the reaction temperature of three-leg DNAzyme walkers on the electrode surface were optimized. The difference (ΔI) of the DPV response in the absence (I_0) and presence (I) of miR-155 ($\Delta I = I_0 - I$) was used for evaluating the performance of the electrochemical biosensor. At first, the reaction time of the TSDR was optimized in the range from 60 to 180 min. As shown in Figure 5A, the electrochemical signal of the reaction system (with target miR-155) decreased with the increase of reaction time and nearly leveled off after 120 min. However, the background signal (without target miR-155) only exhibited a slow decrease when the reaction time exceeded 90 min, suggesting the low cleavage efficiency of single DNAzyme molecules or a low leakage reaction (unprompted self-assembly of H1, H2, and H3) in the designed system.[46,47] Hence, the maximum $|\Delta I|$ is acquired at 120 min, which is selected as the TSDR reaction time.

The effect of SHP concentration on the response of the biosensor was also investigated (Figure 5B). When the concentration of the SHP increased from 0.4 to 1.2 μM, the response current of the system with or without miR-155 increased, and the $|\Delta I|$ reached the maximum at 1 μM. Because more SHPs were immobilized on the electrode surface and more MB could interact with them, a stronger peak current was produced. However, the higher concentration of the SHP than 1 μM was likely to increase the steric hindrances of hybridization between three-leg DNAzyme walkers and the SHP. Consequently, the efficiency of cleaving the SHP declined and the $|\Delta I|$ decreased. Therefore, the optimal concentration of the SHP for this sensing system is 1 μM. Furthermore, according to the previous report,[48] the density of the SHP on the electrode surface is calculated to be 1.6×10^{12} molecules/cm^2. The detailed discussion and Figure S4 are given in the Supporting Information.

Considering the influence of reaction temperature on the catalytic efficiency of the DNAzyme, it is vital to optimize the reaction temperature for the detection of target miR-155. In Figure 5C, we can clearly see that with the increase of reaction temperature, the peak current value of the background

https://doi.org/10.1021/acs.analchem.1c01522
Anal. Chem. 2021, 93, 8962−8970

(without target miR-155) almost remained constant. However, the peak current of the reaction system (with target miR-155) decreased prominently and reached the minimum at 25 °C. When the temperature was higher than 25 °C, the peak current increased instead, which was due to the weakened stability of the DNAzyme at a high temperature.[49] Therefore, 25 °C served as the optimal reaction temperature of DNAzyme walkers.

Analytical Performance of the Electrochemical Biosensor. Under optimal conditions, the DPV response of this biosensor toward different concentrations of the target miR-155 is shown in Figure 6A,B. The DPV response gradually reduced with the increase of the miR-155 concentration from 0 to 1 nM. A good linear relationship of the peak currents and the logarithm of the target miR-155 concentration ranging from 5 fM to 100 pM was observed in the inset of Figure 6B. The linear regression equation of IP (A) = $-4.458 \times 10^{-7} + 4.115 \times 10^{-8}$ lg $C_{miR\text{-}155}$ (R^2 = 0.994) was obtained, and the LOD was as low as 0.27 fM at a signal-to-noise ratio of 3 (S/N = 3). In comparison with the previously reported methods for nucleic acid detection, the proposed sensing strategy based on the TSDR and three-leg DNAzyme walker-mediated amplification strategy showed a lower LOD and a wide linear range (Table S3). Besides, this strategy not only has high sensitivity for detection of miR-155 but also holds the flexibility to detect other target nucleic acids with only needing to design the THP in the main circuit.

Specificity and Reproducibility of the Proposed Biosensor. To investigate the specificity of the proposed biosensor, we compared DPV responses of the biosensor toward miR-155 with other microRNAs, including microRNA-21 (miR-21), microRNA-133a (miR-133a), single-base mismatched microRNA-155 (smiR-155), and triplex-base mismatched microRNA-155 (tmiR-155) under the same experiment conditions. The concentration of other microRNAs were 10 times (10 nM) that of miR-155 (1 nM). As illustrated in Figure 7, the DPV response of other microRNAs (except miR-155) showed slight changes in contrast to the blank (background signal without microRNA). Nevertheless, in the presence of target miR-155, the DPV response had a significant decline, which indicated a good specificity of the biosensor to target miRNA. The DPV response values of smiR-155 and tmiR-155 were nearly 3-fold higher than that of miR-155, demonstrating that the developed biosensor could differentiate the single-base and three-base mismatched sequences from the target sequence. Additionally, five measurements for miR-155 at 100 fM and 10 pM were performed to evaluate the reproducibility of the biosensor, and the relative standard deviations were 1.8 and 2.4%, respectively. The above results attested that the biosensor based on the THP and TSDR to form three-leg DNAzyme walkers could be utilized to specifically and reliably detect the target miR-155.

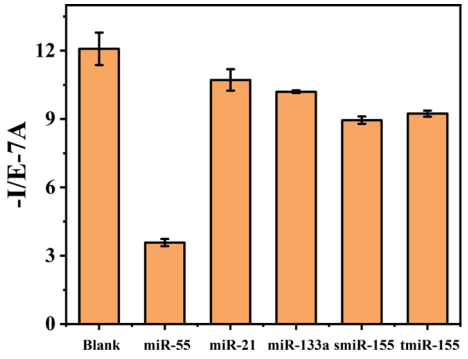

Figure 7. Specificity investigation of the designed biosensor. DPV peak current response to blank, target miR-155, miR-21, miR-133a, and single-/triplex-base mismatched sequences of miR-155, respectively. Error bars show the standard deviation of three measurements.

Detection of miR-155 in a Real Sample. The reliability of the sensing strategy for real sample analysis was examined via testing miR-155 in a biological matrix. Different amounts of miR-155 were spiked into 10% human blood serum samples, and then the total amounts of miR-155 were determined by the method. As exhibited in Table 1, the recovery ranging from 94.1 to 99.8% was obtained with the RSD between 1.2 and 3.7%. The result indicated that the designed sensing strategy has the potential application for target nucleic acid detection in biological samples.

Table 1. Determination Results of miR-155 Detection in 10% Human Serum Samples (n = 5)

sample number	added/pM	detected/pM	recovery (%)	RSD (%)
1	0.050	0.0495	99.0	2.6
2	0.400	0.399	99.8	3.2
3	10	9.575	95.8	1.2
4	100	94.085	94.1	3.7

CONCLUSIONS

In summary, a label-free and universal electrochemical biosensor was constructed for highly sensitive and specific detection of target microRNA. It is the first time to integrate the THP with the TSDR to form the three-leg DNAzyme walkers. Beyond that, the DPI technique was applied to monitor the process of DNA immobilization and reaction on the chip surface, which not only verified the feasibility of the heterogeneous reaction process of the biosensor but also provided the real-time conformational information of the DNA probe. Based on the cyclic utilization of miR-155/THP complexes in the TSDR system, a large number of three-leg DNAzyme walkers were generated, realizing the efficient catalytic cleavage of the SHP on the electrode surface and amplifying the signal of the input miR-155. Hence, the analytical performance of the biosensor was greatly improved, which displayed a high sensitivity with the LOD as low as 0.27 fM for detecting miR-155. Furthermore, the biosensor could differentiate target miR-155 from other microRNA, including the single-base and triple-base mismatched sequences. Also, the practical application of this biosensor was testified by detecting miR-155 in human blood serum samples. In brief, the proposed label-free electrochemical biosensor avoids the costly labeling process and has the potential as a versatile platform for the detection of various target nucleic acids. With the traits of being sensitive, selective, and low-cost, the developed method holds promising potential for application in biomedical research and early diagnosis of diseases.

ASSOCIATED CONTENT

Supporting Information

The Supporting Information is available free of charge at https://pubs.acs.org/doi/10.1021/acs.analchem.1c01522.

https://doi.org/10.1021/acs.analchem.1c01522
Anal. Chem. 2021, 93, 8962−8970

All of the sequences used in the experiment, AFM images of the assembly products in the absence and presence of miR-155, X-ray photoelectron spectroscopy analysis of the elements' change on the electrode surface, fluorescence spectra analysis, chronocoulometric (CC) experiment, layer parameters for the immobilized layer, and comparison of various biosensors for the detection of target nucleic acids (PDF)

AUTHOR INFORMATION

Corresponding Authors

Jianshe Huang − *State Key Laboratory of Electroanalytical Chemistry, Changchun Institute of Applied Chemistry, Changchun, Jilin 130022, China*; Phone: +86 431 85262964; Email: huangjs@ciac.ac.cn; Fax: +86 431 85689278

Xiurong Yang − *State Key Laboratory of Electroanalytical Chemistry, Changchun Institute of Applied Chemistry, Changchun, Jilin 130022, China; University of Science and Technology of China, Hefei, Anhui 230026, China*; orcid.org/0000-0003-0021-5135; Phone: +86 431 85262056; Email: xryang@ciac.ac.cn; Fax: +86 431 85689278

Authors

Yu Xue − *State Key Laboratory of Electroanalytical Chemistry, Changchun Institute of Applied Chemistry, Changchun, Jilin 130022, China; University of Science and Technology of China, Hefei, Anhui 230026, China*

Yu Wang − *State Key Laboratory of Electroanalytical Chemistry, Changchun Institute of Applied Chemistry, Changchun, Jilin 130022, China; University of Science and Technology of China, Hefei, Anhui 230026, China*

Sinuo Feng − *State Key Laboratory of Electroanalytical Chemistry, Changchun Institute of Applied Chemistry, Changchun, Jilin 130022, China; University of Science and Technology of China, Hefei, Anhui 230026, China*

Mengxia Yan − *State Key Laboratory of Electroanalytical Chemistry, Changchun Institute of Applied Chemistry, Changchun, Jilin 130022, China; University of Science and Technology of China, Hefei, Anhui 230026, China*

Complete contact information is available at: https://pubs.acs.org/10.1021/acs.analchem.1c01522

Notes

The authors declare no competing financial interest.

ACKNOWLEDGMENTS

This work was financially supported by the National Natural Science Foundation of China (no. 22034006, 21627808 and 21721003) and the Key Research Program of Frontier Sciences, CAS (QYZDY-SSW-SLH019).

REFERENCES

(1) Victor, A. *Nature* **2004**, *428*, 350−355.
(2) Qing, Z.; Xu, J.; Hu, J.; Zheng, J.; He, L.; Zou, Z.; Yang, S.; Tan, W.; Yang, R. *Angew. Chem., Int. Ed.* **2019**, *58*, 11574−11585.
(3) Panigaj, M.; Johnson, M. B.; Ke, W.; McMillan, J.; Goncharova, E. A.; Chandler, M.; Afonin, K. A. *ACS Nano* **2019**, *13*, 12301−12321.
(4) Wei, Y.; Nazari-Jahantigh, M.; Neth, P.; Weber, C.; Schober, A. *Arterioscler. Thromb. Vasc. Biol.* **2013**, *33*, 449−454.
(5) Pasquinelli, A. E. *Nat. Rev. Genet.* **2012**, *13*, 271−282.
(6) Masaki, S.; Ohtsuka, R.; Abe, Y.; Muta, K.; Umemura, T. *Biochem. Biophys. Res. Commun.* **2007**, *364*, 509−514.
(7) Lukiw, W. J.; Surjyadipta, B.; Dua, P.; Alexandrov, P. N. *Int. J. Biochem. Mol. Biol.* **2012**, *3*, 105−116.
(8) Wang, H.; Wang, H.; Wu, Q.; Liang, M.; Liu, X.; Wang, F. *Chem. Sci.* **2019**, *10*, 9597−9604.
(9) Yang, F.; Cheng, Y.; Cao, Y.; Zhang, Y.; Dong, H.; Lu, H.; Zhang, X. *Anal. Chem.* **2019**, *91*, 9828−9835.
(10) Zhang, J.; He, M.; Nie, C.; He, M.; Pan, Q.; Liu, C.; Hu, Y.; Yi, J.; Chen, T.; Chu, X. *Anal. Chem.* **2019**, *91*, 9049−9057.
(11) Zhu, J.; Ding, Y.; Liu, X.; Wang, L.; Jiang, W. *Biosens. Bioelectron.* **2014**, *59*, 276−281.
(12) Zhang, D. Y.; Winfree, E. *J. Am. Chem. Soc.* **2009**, *131*, 17303−17314.
(13) Zhang, D. Y.; Seelig, G. *Nat. Chem.* **2011**, *3*, 103−113.
(14) Yao, D.; Song, T.; Sun, X.; Xiao, S.; Huang, F.; Liang, H. *J. Am. Chem. Soc.* **2015**, *137*, 14107−14113.
(15) Zhang, D. Y.; Turberfield, A. J.; Yurke, B.; Winfree, E. *Science* **2007**, *318*, 1121.
(16) Zhang, D. Y.; Hariadi, R. F.; Choi, H. M. T.; Winfree, E. *Nat. Commun.* **2013**, *4*, 1965.
(17) Franco, E.; Friedrichs, E.; Kim, J.; Jungmann, R.; Murray, R.; Winfree, E.; Simmel, F. C. *Proc. Natl. Acad. Sci. U.S.A.* **2011**, *108*, No. E784.
(18) Qian, L.; Winfree, E. *Science* **2011**, *332*, 1196.
(19) Guo, Y.; Wu, J.; Ju, H. *Chem. Sci.* **2015**, *6*, 4318−4323.
(20) Bi, S.; Yue, S.; Wu, Q.; Ye, J. *Biosens. Bioelectron.* **2016**, *83*, 281−286.
(21) Li, B.; Chen, X.; Ellington, A. D. *Anal. Chem.* **2012**, *84*, 8371−8377.
(22) Tang, Y. D.; Liu, Y. C.; Lyu, B. Y.; Guo, L. L.; Li, B. L. *Chin. J. Anal. Chem.* **2018**, *46*, 865−874.
(23) Kim, H.-K.; Liu, J.; Li, J.; Nagraj, N.; Li, M.; Pavot, C. M.-B.; Lu, Y. *J. Am. Chem. Soc.* **2007**, *129*, 6896−6902.
(24) Li, Z.; Liu, Y.; Liu, G.; Zhu, J.; Zheng, Z.; Zhou, Y.; He, J. *Bioorg. Med. Chem.* **2014**, *22*, 4010−4017.
(25) Carmi, N.; Balkhi, S. R.; Breaker, R. R. *Proc. Natl. Acad. Sci. U.S.A.* **1998**, *95*, 2233−2237.
(26) Purtha, W. E.; Coppins, R. L.; Smalley, M. K.; Silverman, S. K. *J. Am. Chem. Soc.* **2005**, *127*, 13124−13125.
(27) Li, Y.; Breaker, R. R. *Proc. Natl. Acad. Sci. U.S.A.* **1999**, *96*, 2746−2751.
(28) Yan, T.; Zhu, L.; Ju, H.; Lei, J. *Anal. Chem.* **2018**, *90*, 14493−14499.
(29) Wang, Y.; Wang, Y.; Liu, S.; Sun, W.; Zhang, M.; Jiang, L.; Li, M.; Yu, J.; Huang, J. *Anal. Chim. Acta* **2021**, *1143*, 21−30.
(30) Qing, M.; Xie, S.; Cai, W.; Tang, D.; Tang, Y.; Zhang, J.; Yuan, R. *Anal. Chem.* **2018**, *90*, 11439−11445.
(31) Li, P.; Wei, M.; Zhang, F.; Su, J.; Wei, W.; Zhang, Y.; Liu, S. *Mater. Interfaces* **2018**, *10*, 43405−43410.
(32) Li, F.; Cha, T.-G.; Pan, J.; Ozcelikkale, A.; Han, B.; Choi, J. H. *ChemBioChem* **2016**, *17*, 1138−1141.
(33) Shin, J.-S.; Pierce, N. A. *J. Am. Chem. Soc.* **2004**, *126*, 10834−10835.
(34) Wang, S.; Lu, S.; Zhao, J.; Huang, J.; Yang, X. *ACS Appl. Mater. Interfaces* **2017**, *9*, 41568−41576.
(35) Xue, Y.; Wang, Y.; Wang, S.; Yan, M.; Huang, J.; Yang, X. *Anal. Chem.* **2020**, *92*, 10007−10015.
(36) Wang, Y.; Zheng, Y.; Yang, F.; Yang, X. *Chem. Commun.* **2012**, *48*, 2873−2875.
(37) Yin, P.; Choi, H. M. T.; Calvert, C. R.; Pierce, N. A. *Nature* **2008**, *451*, 318−322.
(38) Farjami, E.; Clima, L.; Gothelf, K. V.; Ferapontova, E. E. *Analyst* **2010**, *135*, 1443−1448.
(39) Wen, J. L.; Chen, J. H.; Zhuang, L.; Zhou, S. G. *Biosens. Bioelectron.* **2016**, *90*, 481−486.
(40) Kelley, S. O.; Barton, J. K.; Jackson, N. M.; Hill, M. G. *Bioconjugate Chem.* **1997**, *8*, 31−37.

(41) He, J.-L.; Zhang, Y.; Mei, T.-T.; Tang, L.; Huang, S.-Y.; Cao, Z. *Biosens. Bioelectron.* **2019**, *144*, 111692.
(42) Escorihuela, J.; González-Martínez, M. Á.; López-Paz, J. L.; Puchades, R.; Maquieira, Á.; Gimenez-Romero, D. *Chem. Rev.* **2015**, *115*, 265−294.
(43) Wang, J.; Xu, X.; Zhang, Z.; Yang, F.; Yang, X. *Anal. Chem.* **2009**, *81*, 4914−4921.
(44) Zheng, Y.; Hu, T.; Chen, C.; Yang, F.; Yang, X. *Chem. Commun.* **2015**, *51*, 5645−5648.
(45) Hu, T.; Wang, S.; Chen, C.; Sun, J.; Yang, X. *Anal. Chem.* **2017**, *89*, 2606−2612.
(46) Jiang, Y. S.; Bhadra, S.; Li, B.; Ellington, A. D. *Angew. Chem.* **2014**, *126*, 1876−1879.
(47) Jiang, Y.; Li, B.; Milligan, J. N.; Bhadra, S.; Ellington, A. D. *J. Am. Chem. Soc.* **2013**, *135*, 7430−7433.
(48) Steel, A. B.; Herne, T. M.; Tarlov, M. J. *Anal. Chem.* **1998**, *70*, 4670−4677.
(49) Li, X.; Xie, J.; Jiang, B.; Yuan, R.; Xiang, Y. *Mater. Interfaces* **2017**, *9*, 5733−5738.

https://doi.org/10.1021/acs.analchem.1c01522
Anal. Chem. 2021, 93, 8962−8970